Design, Control and Analysis of a Dual-arm Continuum Flexible Robot System

Chenxi Wang[1], Zhi Li[1], Yunfan Ren[1], Yuwen Deng[4] and Shuang Song*
School of Mechanical Engineering and Automation, Harbin Institute of Technolgy, Shenzhen, China, 518055

***Abstract*— Multi-arm flexible robot can cooperate with each other to achieve complex surgical actions during operation. In this paper, we propose the mechanical structure design, control and analysis of a dual-arm continuum flexible robot for surgical task that needs multi-tools cooperation. The movement of a single arm is controlled by a set of flexible wires. The two arms work together under control of a remote device to perform actions such as gripping and cutting, which cannot be done with single arm. Kinematic model of the flexible arm has been established. Accuracy of the motion has been tested and verified. Experimental results demonstrate the feasibility of the proposed system.**

***Index Terms*— Dual-arm robot; Flexible Robot; Kinematic Model.**

I. Introduction

Robotic technology has been well developed and widely used among various scenarios. During these applications, medical robot is now becoming one of the hot research topics. Nowadays, abdominal surgery is commonly performed in a narrow environment, which makes it difficult for doctors to make accurate judgments on points that need to be cut. At the same time, long time high-concentration surgical operations can cause occupational fatigue in doctors. For the patients, open surgery will produce large wound which is not conducive to postoperative recovery and can also cause complications. This will not only harm the patient's body, but also affect the patient's psychology. Therefore, a minimally invasive surgical robot with accuracy and stability is required. Surgical robot that currently meets the requirements is Da Vinci Robot, but it has the disadvantage of a large area and expensive construction. Due to the surgeon's requirements for precision and convenience of surgery and people's requirements for reducing the pain of abdominal and oral diseases, continuum flexible robot has been widely studied and designed [1].

Jan Peirsa et al designed a flexible robot with two degrees of freedom [2]. It consists of four ropes and a nickel-titanium alloy tube. Each degree of freedom is controlled with two ropes. Therefore, robot can be controlled to move by pulling the ropes. Xu proposed a flexible robot which used four nickel-titanium alloy tubes as the skeleton for minimally invasive surgery. However, its diameter is 7.5mm, which makes it not thin enough for working in a narrow space [3]. Dong-Geol Choi et al designed a spring-based microscopic endoscope [4][5]. Nabil Simaan invented a Snake-like units using flexible backbones [6]. The difference between this robot and other surgical robots is that it uses only a single flexible skeleton and a line-driven working method, which is more suitable for minimally invasive surgery in the throat and other parts.

Nowadays, most of wire-driven flexible robots only have a single arm [7]–[9], which makes it difficult to solve complex problems in the abdominal and oral surgeries when multi-tools cooperation is needed. In this paper, we proposed a wire-driven flexible robot model with two arms for collaboration application. In this way, simultaneous clamping and cutting in the abdominal cavity and the oral cavity can be achieved. In addition, the two arms collaborate with each other can also achieve suture surgery. But such a design creates a requirement for the size of the robot, since the gut has two or more robot arms at the same time. Therefore, we reduced the diameter to five millimeters with a novel design. This size is sufficient for complex work in a narrow environment. In addition, we designed the optimal angle for extending the arms to expand work space. A kinematics model and a workspace model of the robot are developed based on the piecewise constant curvature assumption in this paper [10]. In this way, forward kinematic model of the robot has be established. Working space has been analyzed with MATLAB.

The rest of the paper is organized as follows: Section II presents the design of the robot and the wire-driven mechanism. Section III gives the kinematics of the continuum robot. Section IV presents the experiments and discussion. Finally, conclusion is drawn in Section V.

II. Design of the Dual-arm Robot System

As shown in Fig. 1, the dual-arm robot is composed of two single arm structures which adopt modular design. Every part is replaceable thanks to modular design. As a result, the dual-arm robot can carry different surgical instruments, which makes it flexible for different combinations. Fig.2 shows the single arm design. Each single arm structure has four degrees

*Correspongding author: S. Song (songshuang@hit.edu.cn)

This work was supported in part by National Key R&D Program of China (2018YFB1307700), in part by National Natural Science Foundation of China (61803123), and in part by the Science and Technology Innovation Committee of Shenzhen (JCYJ20170413110250667).

of freedom of mechanism. The arm can be controlled to move forward and backward, left and right, up and down. Nickel-titanium composite wire is used to driven the movement due to its stiffness and flexibility. Moreover, a revolve mechanism is integrated at the bottom to adjust the angle between two arms.

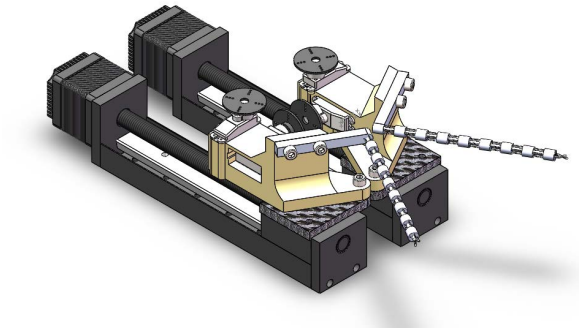

(a)

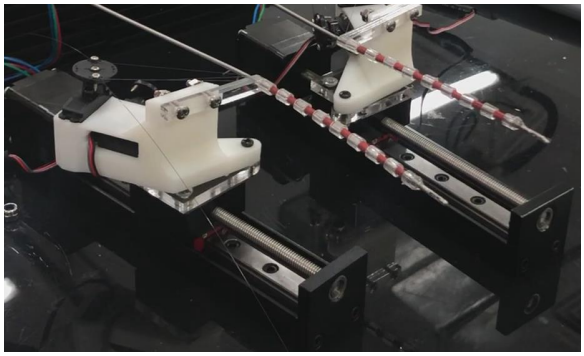

(b)

Fig. 1. The proposed dual-arm structure. It is composed of two single arm structures which adopt modular design. (a) 3D model of the proposed robot system; (b) the manufactured dual-arm robot system.

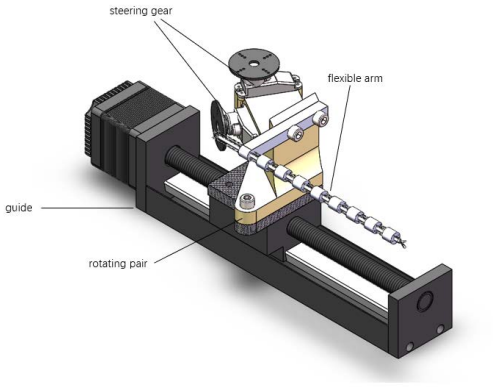

Fig. 2. The designed single arm structure.

The designed robot is for nasal cavity, which has a length about 13cm, and the width of the nasal cavity is about 1cm.

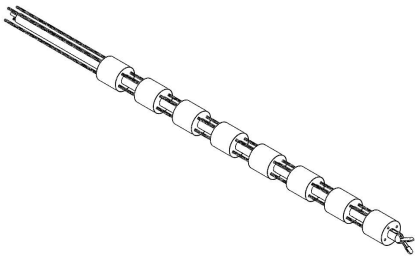

(a) Schematic diagram of a single arm with wires and end effector.

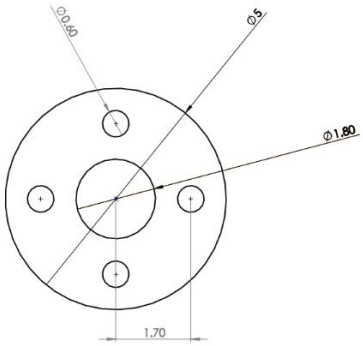

(b) Surface chart of a single joint.

Fig. 3. Schematic diagram of a single arm with wires and end effector. To achieve a miniature design, each arm contains 8 joints. Each joint is 5mm in diameter and 5mm in length.

To achieve a miniature design, each arm contains 8 joints. As shown in Fig. 3, each joint is 5mm in diameter and 5mm in length and the distance between each two joints is 5 mm. The middle round hole passes through a flexible tube loaded with surgical end effectors. Four small holes penetrate the flexible rope which is made of Nickel-titanium composite wire. The flexible rope can be pulled by the rotation of the rudder, which makes the flexible pipe bend.

In order to increase the working radius as much as possible and the meantime it can enter the nasal cavity, the initial angle of the two arms is set to be 15°. As shown in Fig. 4, the maximum angle of the arms is 60°. The initial distance is 1cm.

In addition, the designed robot can be updated to a three-arm structure due to its modular design, which can be seen in Fig. 5. The ends of the three arms are on the same plane, and the wires can form an equilateral triangle. The distance between the ends of the arms is different depending on the use. It can include two flexible arms with surgical instruments and a flexible arm with a camera.

The whole circuit is powered by 24V DJI high-performance lithium batteries. With 24V to 5V and 24V to 7.4V adapters, all components can be powered from the same

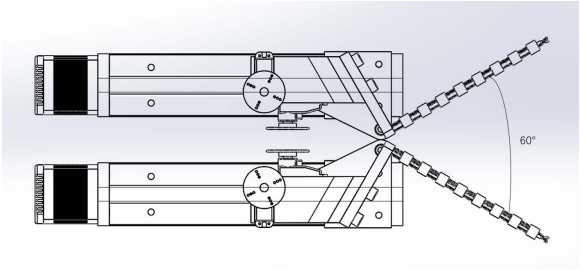

Fig. 4. Schematic diagram of the two arms when there is an angle between each other.

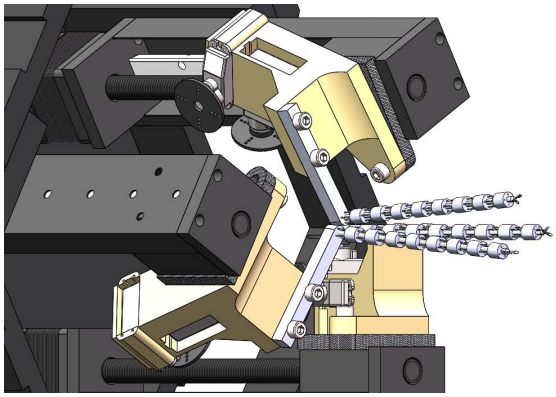

Fig. 5. The designed robot system can update to a three-arm structure.

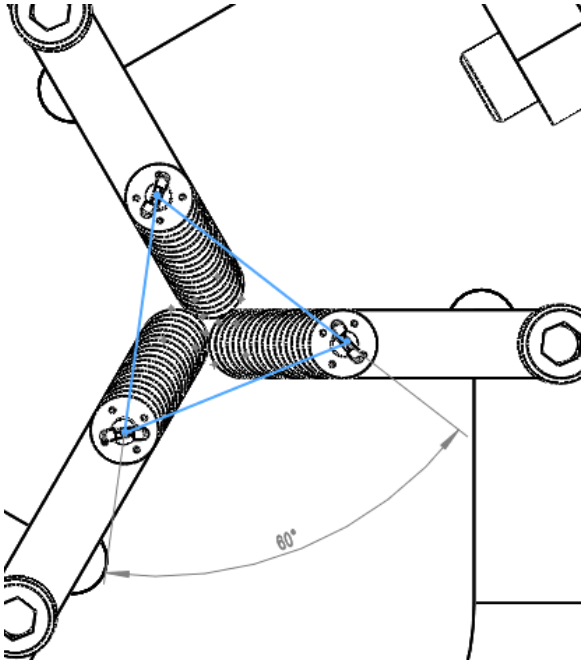

Fig. 6. Angle between three robot arms.

source. STM32 MCU is used as the controller for the flexible arms. For each arm, a stepper motor is applied to drive the screw slide to ensure the accuracy and stability of the forward and backward movement. Inservos's miniature digital servo D0474HR-HV is used to achieve precise position servo control of the wires to achieve swing movement. A Remote controller with multiple channels is used for operators to control the robot. As shown in Fig. 7, after receiving the movement command, the remote controller sends the signal to the MCU through the serial port signal. After receiving the signals, MCU converts the movement command to motor control information according to the kinematic model. Then, the stepping motor will be controlled by a single pulse to realize the forward and backward movement of the robot arm. Through the PWM control method, the servo is controlled to pull the Nitinol wire to realize the UDRL movement of the robot arm.

III. Kinematics Model and Workspace Analysis

The Kinematics model and workspace model of the robot are developed based on the piecewise constant curvature assumption in this paper. According to our previous work [11], we have the following model

$$x^2 + y^2 + (z - H_S - H_E)^2 = \\ -2H_E \times cos\frac{(N+1)\theta}{2} - (H + h_0)\frac{sin(\frac{N\theta}{2})}{sin\frac{\theta}{2}} \quad (1)$$

In order to achieve fully cooperation between the two robot arms, optimal angle for extending the arms to expand work space needs to be determined. First the two arms are placed in parallel along the X-axis with a spacing of d (set to 50mm). According to the kinematic model of the flexible robot, working space of each flexible robot arm can be obtained. However, if the propulsion distance of the flexible robot is changed within a certain range, the discrete point area will be greatly increased. To simplify the analysis, the propulsion distance s is set to be invariant, and the propulsion distances of the two flexible robots are always equal. Therefore, the end discrete points of the two arms' tip constitute two curved surfaces similar to ellipsoids. When α(which is defined in Fig. 8)changes, the intersection of the two surfaces also changes.

When the distance between discrete points on the two surfaces is less than 1 mm, the pair of discrete points is marked as the intersection area. By traversing α in a certain range to obtain the number of discrete points in the intersection area, we aim to find a result that the actual two flexible robots have the maximum workable area when working (the distance between the two ends does not exceed a certain distance).

Fig. 9 shows the case where α changes from 0° to 30°, $d = 50mm$, $H = 5mm$, $H_0 = 4$, $H_E = 13$, $N = 8$, and the maximum angle between each point is 5°.

It can be seen from the Fig. 9 that when α is around 15° to 20°, the number of discrete points representing the

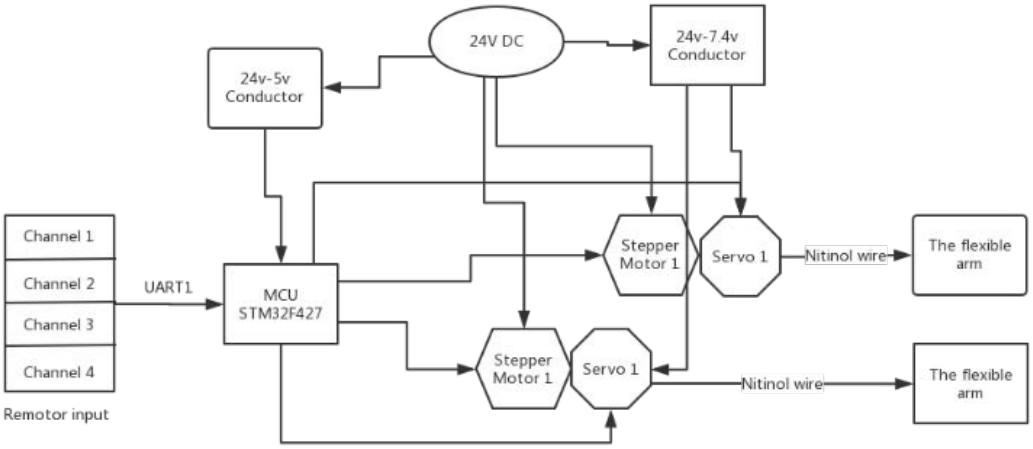

Fig. 7. Schematic diagram of remote control of the proposed robot system.

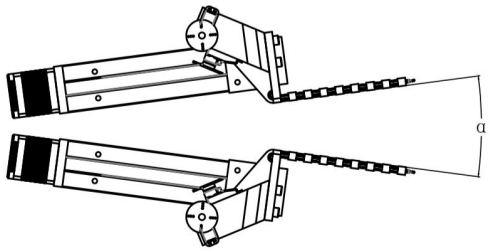

Fig. 8. The explanation of α.

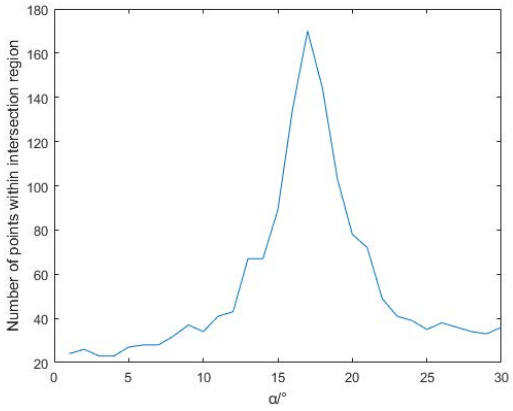

Fig. 9. Number of intersection points with varying angle α, with a step of 5°.

volume of the intersection area is abrupt, which is probably caused by the error generated when the discrete point data is generated, indicating the step size of the discrete point is not small enough. After reducing the step size, the result is as follows:

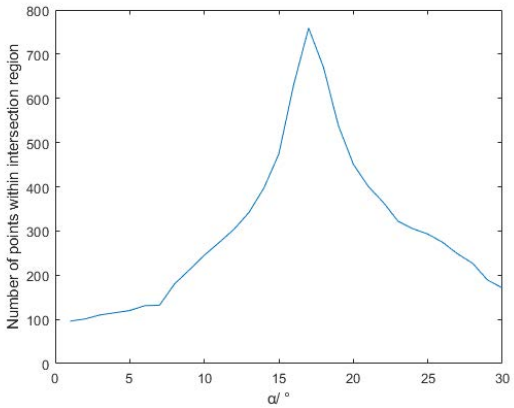

Fig. 10. Number of intersection points with varying angle α, with a step of 1°.

The comparison shows that although the accuracy is increased and more dense end position data points are generated, the intersection area size and the angle α are approximately the same, and the optimum angle α is still between 15° and 20°. The three-dimensional result of the discrete points is shown in Fig. 11 when $\alpha = 15°$. Black points represent the points that belongs to the intersection of the workspace. It can be seen that the step length of the generated discrete points is large, which causes the dots to be too scattered, thus causing the black dots to be uneven and not forming the continuous lines that should be formed. However, as shown in Fig. 9 and Fig. 10, improving the step

accuracy does not affect the qualitative analysis results.

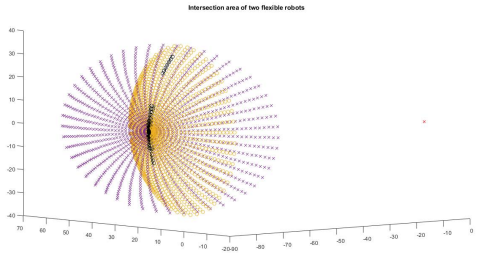

Fig. 11. Workspace analysis. Black represents the point that belongs to the intersection of the two arms.

IV. Experiments

A. Path Following Experiment

In this experiment, the robot arm is controlled to follow a circle path, which can be seen in Fig. 12.

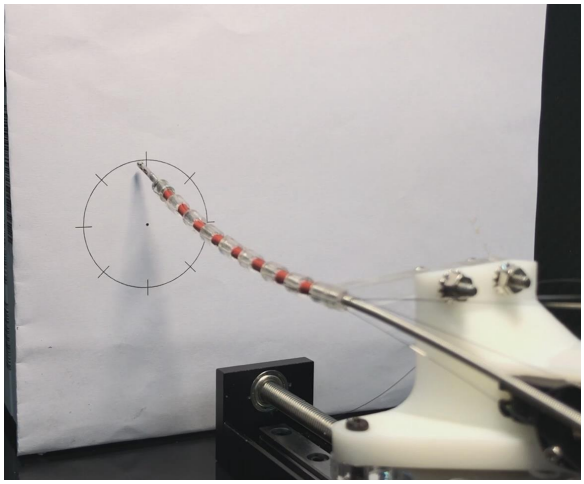

Fig. 12. Circle path following experiments.

Before the experiment, a circle with a 50mm diameter has been drew on a paper to serve as a reference. The robot tip is first placed at the center of the circle, and then controlled to move follow the circle. A following result is shown in Fig. 14. Fig. 15 shows the trace result, which is defined as the distance between the arm tip and the center of the reference circle. Fig. 16 shows the trace error. The average trace error is 0.7mm, with a standard deviation of 0.6mm.

To record the position data each point, we use a camera which record 25 frames per second. Place the arm, a transparent acrylic plate with the reference circle and the camera as shown in the Fig. 14.We play the recorded video frame by frame and record the position of the end every five frames.Then we can get some records like Fig. 14. In fact, due to the parallax effect of the camera, there will be a difference between the recorded path and the real path. We put the axis of the camera and the axis of the arm (zero position) on one line, and place the camera a little further, so that we can basically ignore the impact of parallax.

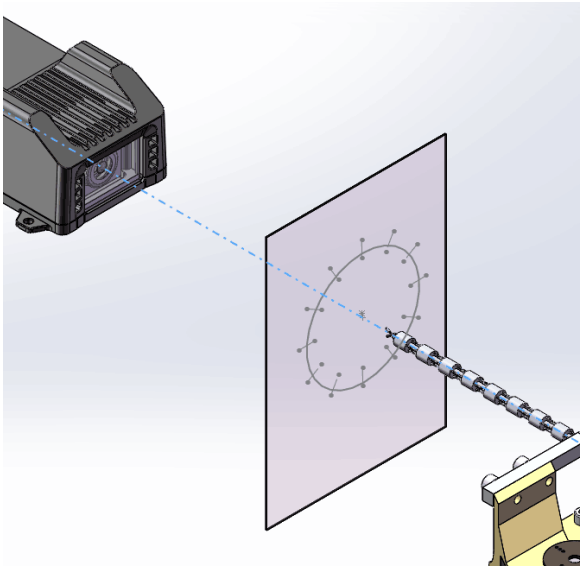

Fig. 13. Record the motion track with the camera.

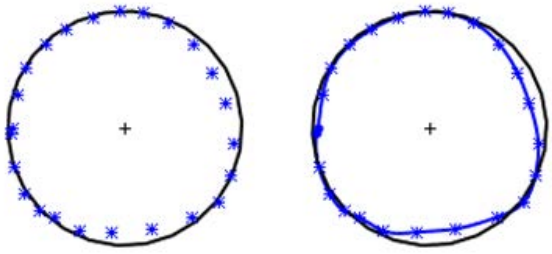

Fig. 14. The circle path following results for one trial.

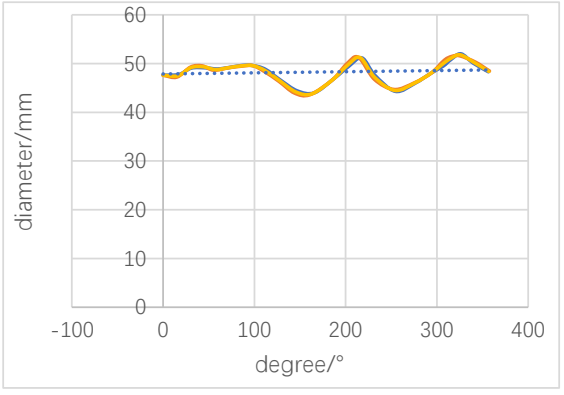

Fig. 15. The circle path following trace result, which is defined as the distance between the arm tip and the center of the reference circle.

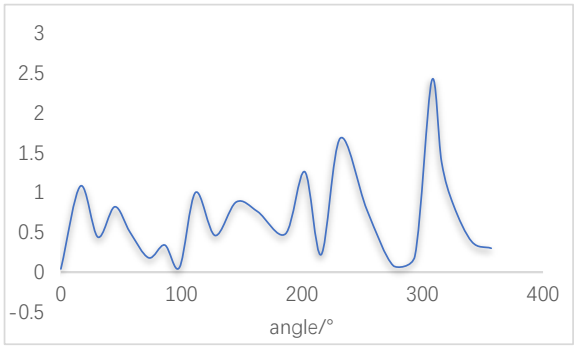

Fig. 16. The circle path following trace error. The average trace error is 0.7mm, with a standard deviation of 0.6mm.

B. Phantom Experiment

Experiment of scenario simulation As shown in Fig. 17, a rubber if fixed in a model of human skull to simulates soft tissue. The two arms go through nasal cavity to do the tissue sampling operation. When reach the tissue, the two arms work together to do the sampling and retreat from the cavity after the sampling has been finished.

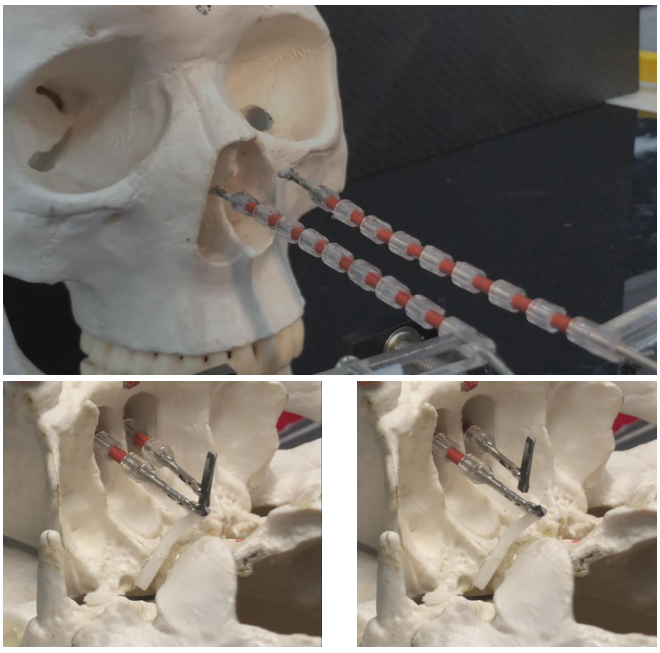

Fig. 17. Phantom experiments. A rubber if fixed in a model of human skull to simulates soft tissue. The two arms go through nasal cavity to do the tissue sampling operation. When reach the tissue, the two arms work together to do the sampling and retreat from the cavity after the sampling has been finished.

C. Discussion

Through the above results, we can observe that although the path following result is acceptable in average error, the control accuracy is still need to be improved. This may caused by the elasticity of the traction wires, as well as the friction between the wire and the joints. These disturbance can not be seen from the kinematics model, which will result in an unpredictable error in real applications, both in tip control and shape control. Therefore, on one hand, material of the wire needs to be chosen accordingly to reduce the elastic error, as well as the frictions though joint design and fabrication; on the other hand, real time shape and tip monitor method should be added to provide better and safer performance.

In the remote control, only the tip can be controlled. Although follow the leader method can be applied, collision may still accrue between the arms during cooperation. Therefore, motion planning for multi-arm cooperation with no collision should be studied in the future.

V. Conclusion

In this paper, we proposed the mechanical structure design, control and analysis of a dual-arm continuum flexible robot for surgical task that needs multi-tools cooperation. Kinematic model of the flexible arm has been established, and the working space has been analysed. Trace following experiments and phantom experiment have been carried out to verify the proposed system. Experimental results demonstrate the feasibility of the proposed system. In the future, we will further improve the performance of the system and carry out motion planning for multi-arm cooperation with no collision.

References

[1] H. Ren, C. M. Lim, J. Wang, W. Liu, S. Song, Z. Li, G. Herbert, Z. T. H. Tse, and Z. Tan, "Computer-assisted transoral surgery with flexible robotics and navigation technologies: A review of recent progress and research challenges," *Critical Reviews in Biomedical Engineering*, vol. 41, no. 4-5, pp. 365–391, 2013.

[2] J. Peirs, H. V. Brussel, D. Reynaerts, and G. D. Gersem, "A flexible distal tip with two degrees of freedom for enhanced dexterity in endoscopic robot surgery," 2002, pp. 271–274.

[3] K. Xu and N. Simaan, "An investigation of the intrinsic force sensing capabilities of continuum robots," *IEEE Transactions on Robotics*, vol. 24, no. 3, pp. 576–587, June 2008.

[4] Dong-Geol Choi, Byung-Ju Yi, and Whee-Kuk Kim, "Design of a spring backbone micro endoscope," in *2007 IEEE/RSJ International Conference on Intelligent Robots and Systems*, Oct 2007, pp. 1815–1821.

[5] Hyun-Soo Yoon and Byung-Ju Yi, "A 4-dof flexible continuum robot using a spring backbone," in *2009 International Conference on Mechatronics and Automation*, Aug 2009, pp. 1249–1254.

[6] N. Simaan, "Snake-like units using flexible backbones and actuation redundancy for enhanced miniaturization," in *Proceedings of the 2005 IEEE International Conference on Robotics and Automation*, April 2005, pp. 3012–3017.

[7] S. Song, Z. Li, H. Yu, and H. Ren, "Electromagnetic positioning for tip tracking and shape sensing of flexible robots," *IEEE Sensors Journal*, vol. 15, no. 8, pp. 4565–4575, Aug 2015.

[8] S. Song, Z. Li, M. Q. . Meng, H. Yu, and H. Ren, "Real-time shape estimation for wire-driven flexible robots with multiple bending sections based on quadratic bézier curves," *IEEE Sensors Journal*, vol. 15, no. 11, pp. 6326–6334, Nov 2015.

[9] Z. Li and R. Du, "Design and analysis of a bio-inspired wire-driven multi-section flexible robot," *International Journal of Advanced Robotic Systems*, vol. 10, no. 4, pp. 1–11, 2013.

[10] M. Gouttefarde, D. Daney, and J. Merlet, "Interval-analysis-based determination of the wrench-feasible workspace of parallel cable-driven robots," *IEEE Transactions on Robotics*, vol. 27, no. 1, pp. 1–13, Feb 2011.

[11] S. Song, C. Zhang, L. Liu, and M. Q.-H. Meng, "Preliminary study on magnetic tracking-based planar shape sensing and navigation for flexible surgical robots in transoral surgery: methods and phantom experiments," *International Journal of Computer Assisted Radiology and Surgery*, vol. 13, no. 2, pp. 241–251, Feb 2018. [Online]. Available: https://doi.org/10.1007/s11548-017-1672-8